



THE UNIVERSITY *of* EDINBURGH

Edinburgh Research Explorer

A CFD-based wing sail optimisation method coupled to a VPP

Citation for published version:

Viola, IM, Biancolini, ME, Sacher, M & Ubaldo, C 2015, 'A CFD-based wing sail optimisation method coupled to a VPP', Paper presented at 5th High Performance Yacht Design Conference, Auckland, New Zealand, 9/03/15 - 11/03/15.

Link:

[Link to publication record in Edinburgh Research Explorer](#)

Document Version:

Peer reviewed version

General rights

Copyright for the publications made accessible via the Edinburgh Research Explorer is retained by the author(s) and / or other copyright owners and it is a condition of accessing these publications that users recognise and abide by the legal requirements associated with these rights.

Take down policy

The University of Edinburgh has made every reasonable effort to ensure that Edinburgh Research Explorer content complies with UK legislation. If you believe that the public display of this file breaches copyright please contact openaccess@ed.ac.uk providing details, and we will remove access to the work immediately and investigate your claim.



A CFD-BASED WING SAIL OPTIMISATION METHOD COUPLED TO A VPP

Ignazio Maria Viola¹, i.m.viola@ed.ac.uk
Marco Evangelos Biancolini², biancolini@ing.uniroma2.it
Matthieu Sacher³, matthieu.sacher@ecole-navale.fr
Ubaldo Cella⁴, ubaldo.cella@designmethods.it

Abstract. An aerodynamic numerical optimisation procedure for an AC72 rigid wing sail was developed. The core of the method is the geometric parameterisation strategy based on a mesh morphing technique. The morphing action, which uses radial basis functions, is integrated within the Reynolds-averaged Navier-Stokes solver and provides an efficient parametric sail aerodynamic analysis method which is integrated in an optimisation environment based on a velocity prediction program. A hydrodynamic model is coupled to the parametric numerical solver in an iterative procedure. The shape modifiers operate on angle of attack and twist of the fore and aft wing element. For each true wind condition, the velocity of the boat is maximised by iterating between the solution of the velocity prediction program and the solution of the fluid dynamic solver. The effectiveness of the proposed method is demonstrated testing a range of wind speeds.

NOMENCLATURE

δ	Angle between main and flap chord (deg)
Δx_{gap}	Gap between wing elements along the main longitudinal axis
Δy_{gap}	Gap between wing elements perpendicular to the main longitudinal axis
γ	Deflection of the main trailing edge (deg)
λ	Leeway angle (deg)
AoA	Angle of attack, between the main element axis and the apparent wind direction (deg)
AR	Aspect ratio
AWA	Apparent wind angle (deg)
AWS	Apparent wind speed (m/s)
B	Boat beam (m)
V_S	Boat speed (m/s)
c	Wing chord (m)
C_{Df}	Foil drag coefficients
C_{Lf}	Foil lift coefficients
D_f	Foil drag (N)
F_{Xw}	Wing sail force component along X axis (N)
F_{Yw}	Wing sail force component along Y axis (N)
g	Gravitational acceleration (m/s ²)
h_f	Hydrofoil centre of pressure distance from waterplane (m)
h_w	Wing centre of pressure distance from waterplane (m)
L_{Yf}	Hydrofoil lift components along Y axis (N)
L_{Zf}	Hydrofoil lift components along Z axis (N)
m	Boat mass (kg)
TWA	True wind angle (deg)
TWS	True wind speed (m/s)
U	Non-dimensional flow velocity

1. INTRODUCTION

This paper describes a shape design tool, suitable for rigid wing sails, which couples a Reynolds-averaged Navier-Stokes (RANS) solver with a Velocity Prediction Program (VPP) within a numerical optimisation environment. The code was developed for an AC72 double element wing configuration. A shape parameterisation strategy, based on a mesh morphing techniques, was employed. The mesh morphing is based on Radial Basis Functions (RBF). This approach allows for the solution of both the geometric parameterisation problem and the computational domain adaptation. An aerodynamic polar formulation was used to model the foil hydrodynamic forces. The boat equilibrium system of equations is solved by iterating between the VPP and the RANS solution. This coupling is integrated with a single-objective numerical optimisation procedure.

RBF are a class of interpolation functions that can be used to drive mesh morphing of the discretised domain of computational models by applying predefined displacements to a set of purposely generated points, called source points. The main characteristics of this approach are:

- Morphing requires significantly less computational time than re-meshing
- Preservation of mesh consistency and topology
- Low disk usage
- Exact control of node position
- Low remeshing noise
- Can be integrated in the computational fluid dynamic solver
- Capable of handling large grids

Despite all aforementioned benefits there are still some open issues that are limiting the potentials of RBF mesh morphing. The first limit is given by mesh distortion

¹ Lecturer, Institute for Energy Systems, School of Engineering, University of Edinburgh, UK.

² Assistant Professor, Department of Enterprise Engineering, University of Rome Tor Vergata, Italy

³ PhD Student, Naval Academy Research Institute, IRENav, Ecole Nationale Supérieure d'Arts et Métiers, Paris, France

⁴ Senior Research Engineer, Design MethodsTM (www.designmethods.aero), Messina, Italy

occurring after morphing. Even if it can be alleviated using smooth morpher (e.g. RBF based on bi-harmonic kernel), there are applications where reusing the same mesh for topological or room reasons is impractical (i.e. too much compression or stretching). The second limit is the high computational cost of RBF. In fact, while at each iteration the mesh is morphed with minimal computational time, the RBF fitting, which is performed just one time to build the parameterisation, is computationally intensive. This can be overcome using fast solvers whose implementation can be delicate and complex. In previous years [1, 2], the high numerical cost has limited the application of RBF. In fact the direct solution grows by N^3 , where N is the number of RBF source points. A recent study about mesh morphing using tri-harmonic RBF kernel [3] demonstrates the good potential of the method, but even in this case performance was perceived as a barrier. The first industrial implementation of RBF mesh morphing was introduced in 2009 [4] where a fast RBF solver for the bi-harmonic kernel, *RBF Morph*, was employed, showing a scalability with $N^{1.6}$. A complete description of the method is given in [5].

Mesh morphing techniques based on RBF Morph was used to deal with several problems as shape optimisation [6], ice accretion simulation [7] and fluid-structure interaction [8]. Industrial applications include: automotive [9], motorsport [10, 11], nautical [12], medical [13] and aerospace [14, 15].

In the 34th America's Cup all teams adopted two-element wings, similar to an aircraft single slotted flap wing configuration with symmetric airfoils. The forward element, also called the main element, may have a flexible trailing edge that introduces camber and provides an additional control system. The rear element is also called the flap.

The AC72 Class Rules regarding the wing are hereby summarised. The rules refer to the wing measurement grid reported in [16]:

- The wing shall be designed to be symmetrical about the wing centreplane in wing measurement position
- The wing is divided into 12 parts with a limitation on the maximum and minimum chord
- The total wing area in measurement position shall not be greater than 260.00 m² nor less than 255.00 m²
- When viewed perpendicular to the wing base plane, the projected area of the wing shall not exceed:
 - 2.25 m² above 33.850 m from the wing base plane
 - 5.50 m² below 2.000 m from the wing base plane
- The leading edge of the wing shall be straight below 8.300 m from the wing base plane

According to these rules, assuming the maximum reference surface and a span ranging from 36.5 m and 38 m, the possible wing aspect ratio ranges between around 10.2 and 11.1. In Figure 1 the maximum and minimum wing planform limits, imposed by the rules, are showed by red and blue curves respectively. Within these limits, the planforms with the maximum and minimum aspect ratio (with constant reference surface) are plotted with thick black lines in Figure 1a and Figure 1b, respectively.

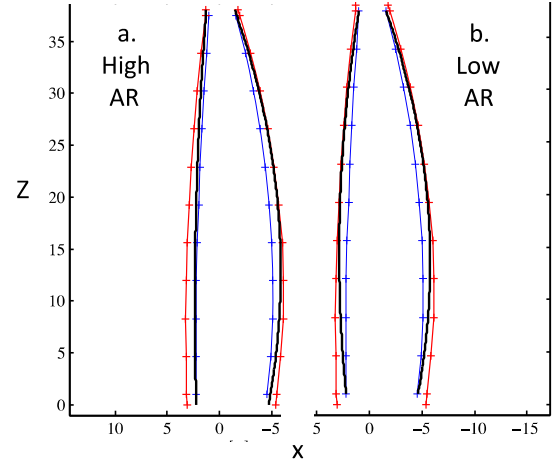


Figure 1. Side view of different aspect-ratio planforms

2. 2D SECTION ANALYSIS

In order to identify the optimum gap between the wing elements, a set of preliminary parametric 2D aerodynamic analyses were performed. Figure 2 shows, as example, the non-dimensional velocity (ratio between the local flow velocity and the free stream velocity) for two positions of the flap with respect to the main element. The angle of attack is $\text{AoA}=11^\circ$ and the flap angle relative to the main element is $\delta=7^\circ$. The distances, along the main element chord, between the trailing edge of the main and the leading edge of the flap (Δx_{gap}) are, in this analyses, $0.02c$ (Figure 2a) and $0.04c$ (Figure 2b). Figure 2 shows that the smaller Δx_{gap} allows an attached boundary layer on the suction side of the flap, and thus higher performance, while the higher Δx_{gap} leads to a stalled flap and to lower performance.

Figure 3 shows how the flap separation can be avoided also deflecting the trailing edge of the main element and thus decreasing the gap between the two wing elements. The contours of non-dimensional velocity are shown for $\text{AoA}=2^\circ$ and $\delta=20$. While Figure 3The use of a flexible trailing edge to control the gap between the elements showed good potentialities but introduced additional variables and complexities and therefore it will not be considered in the following 3D analysis.

The optimum range of flap position and deflection resulting from this parametric study are summarised in Table 1. Interested readers can find a dissertation on 2D high lift device design in [17].

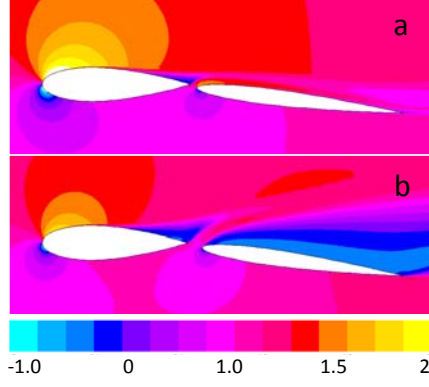


Figure 2. Contours of U for $\Delta x_{gap} = 0.02c$ (a) and $\Delta x_{gap} = 0.04c$ (b)

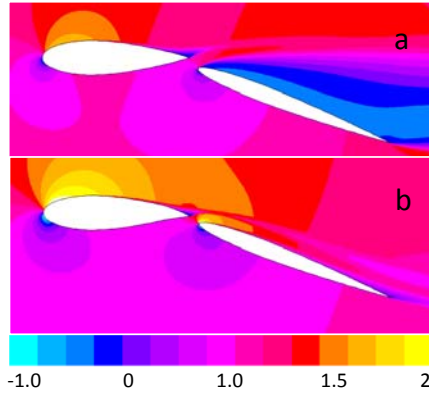


Figure 3. Contours of U for $\gamma = 0^\circ$ (a) and $\gamma = 10^\circ$ (b)

Table 1. Optimum 2D parameters

Δx_{gap}	$0.02c - 0.03c$
Δy_{gap}	$0.015c - 0.025c$
γ	$\sim \frac{\delta}{2}$

3. 3D ANALYSIS

The proposed algorithm couples the RANS solver with the VPP in an optimisation environment. The objective function of the optimisation is the maximum boat speed along the sailed course (V_S). The maximum aspect ratio planform and the optimum gap between wing elements without main trailing edge deflection were adopted to define the 3D geometry.

3.1 Wing trim

The vertical profile of the angle of attack of the main and flap elements are defined by a 2D quadratic Bézier curves (Figure 4). The first control point, located at the root section, has as abscissa the reference element angle of attack. The mid point controls the shape of the twist profile. This results in four degrees of freedom per wing element: the angle of the three points and the height of the mid point. However, the same height and angle were

used for the mid control points of the two elements, leading to six parameters in total. It was found that the computational time required to optimise all six parameters with a standard workstation was impractical. Therefore, in the results presented here, for each iteration the twist is set to match that of the updated apparent wing angle vertical profile, while the root angle of attack of the main element (AoA) and the root deflection of the flap (δ) are optimised.

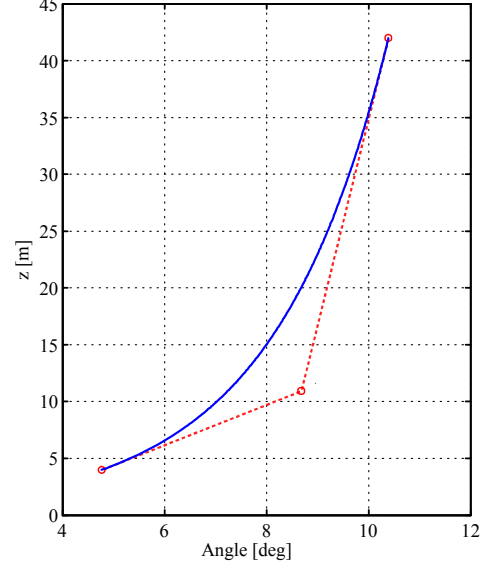


Figure 4. Example of twist distribution defined by three points

3.2 Mesh morphing

Mesh morphing and shape parameterisation are performed with RBF Morph. The range of grid nodes displacement is set a priori and the morphing is controlled by source points, which define the dimension of the RBF problem. The mesh morphing is performed in two steps: the nodes of the moving walls are first moved according to the defined kinematics, the RBF action is then extended in the volume, smoothing the grid up to the prescribed surrounding limits. The obtained RBF solution is sent to the RANS solver.

3.3 RANS

The domain is made of a cube, whose faces are 30 m from the wing in all directions, but for the bottom face that models the water plane. The wing is fixed and the twisted apparent wind velocity profile is used as a Dirichlet boundary condition on the two upstream faces, symmetry condition is used on the bottom and top face, while a Neumann condition for the pressure is applied on the two downstream faces. A coarse multi-block structured hexahedral grid (Figure 5) with only 200.000 cells is used to demonstrate the effectiveness of the proposed method, however it is anticipated that a finer grid would be necessary to decrease the numerical uncertainty. Future works should include the quantification of the uncertainty of the computations, and the propagation of the RANS uncertainty on the

optimised solution. This analysis should provide the requirements, including grid and time step resolution, and convergence criteria, for the specific design purpose. The rig and the hull are not modelled in the present simulations but these should be included for industrial applications of the proposed method.

The incompressible steady RANS equations for Newtonian fluids are solved together with the two equation $k-\omega$ Shear Stress Transport (SST) turbulence model [18]. A steady pressure-based solver, with a coupled scheme for pressure-velocity coupling, and second order upwind scheme for spatial discretisation is adopted.

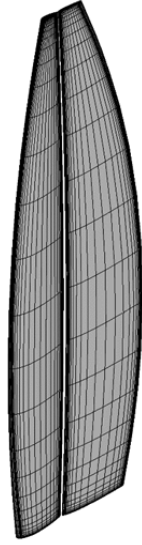


Figure 5. Surface grid of the wing

3.4 VPP

The boat is modelled as flying upright on the leeward foil and the equilibrium is computed for four degrees of freedom, pitching and yaw moments excluded. Figure 6 shows the equilibrium of boat in the front plane and the equilibrium of the forces.

The system of equilibrium, assuming the X axis aligned to the boat direction, is:

$$(S) = \begin{cases} F_{x_w} = D_f \\ F_{y_w} = L_{y_f} \\ mg = L_{z_f} \\ F_{y_w}(h_w + h_f) - mgb_f = 0 \end{cases} \quad (1)$$

where F_{x_w} and F_{y_w} are the sail aerodynamic forces along the X and Y axis, respectively; D_f is the hydrofoil drag; L_{y_f} and L_{z_f} are the hydrofoil lifts in the side and vertical direction, respectively; h_w and h_f are the distances from the water plane of the centre of pressure of the wing and hydrofoil, respectively; b_f is the distance between the

centre of pressure of the hydrofoil and the boat's symmetry plane; and mg is the gravitational force.

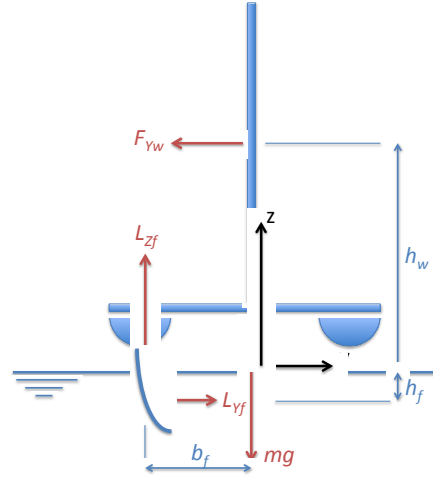


Figure 6. Schematic diagram of the boat equilibrium

The hydrodynamic forces are computed using 2D foil experimental coefficients and potential flow theory, assuming that the hydrofoils are isolated symmetrical elliptical untwisted wings [19]. The lift and drag coefficients can therefore be computed as:

$$C_{D_f} = C_{D_{f0}} + \frac{C_{L_f}^2}{\pi AR_f} \quad (2)$$

$$C_{L_f} = \frac{C_{L_{f0}}}{1 + \frac{2}{AR_f}} \quad (3)$$

where C_{L_f} and C_{D_f} are the lift and drag coefficients of the hydrofoil; $C_{L_{f0}}$ and $C_{D_{f0}}$ are the 2D lift and drag coefficients of the hydrofoil section taken from experimental database; and AR_f the aspect ratio of the hydrofoil.

The process is led by Matlab scripts that drive the RANS solver, extract the aerodynamic forces, solve the equilibrium equations of the VPP, run the optimisation algorithm, update the RANS boundary conditions and repeat the cycle until convergence is reached. Figure 7 shows the workflow of the procedure. The objective is to find the trim that maximises the boat speed (V_S) at fixed true wind speed (TWS) and angle (TWA). The process starts guessing V_S , h_f , the leeway angle (λ) and a wingsail trim. The apparent wind speed profile is computed and imposed as the RANS boundary conditions. When the RANS simulation is converged, the time-averaged forces acting on the wing are extracted and used to solve the system (S), which provides new values of V_S , λ and h_f . The boat speed is estimated by an iterative procedure in which an optimisation criterion, based on the Nelder-Mead Simplex algorithm [20], finds the optimum h_f and leeway angle λ that maximise the

boat speed and satisfy the constraint $F_{Y_w} - L_{Y_f} = 0$. The RANS simulation is run again updating the onset velocity profile based on the computed V_s , λ and h_f . Convergence is achieved when the absolute value of the difference between the latest two computed boat speeds, V_s^n and V_s^{n+1} , respectively, is smaller than an acceptable error ϵ .

The routine is implemented with the possibility to select, as optimisation criterion, between a pattern search [21] and a genetic algorithm [22].

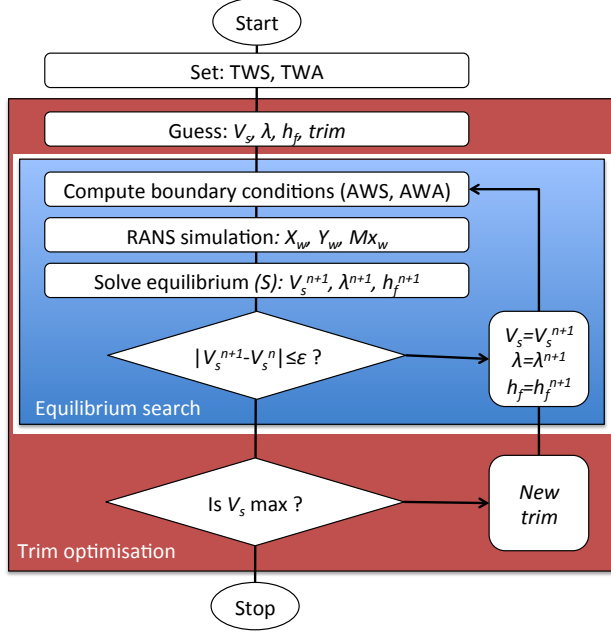


Figure 7. Program flowchart

3.5 Examples of results

To demonstrate the potentialities of the presented method, the program was run for a true wind angle of 50° and for true wind speeds of 10 knots and 15 knots.

The main trailing edge and the flap leading edge were maintained straight and parallel, and the gap between the elements was set constant along the span to 2% of the chord (Fig. 8). The twist profile was set equal to the vertical profile of the apparent wind angle, which was calculated every iteration of the “Equilibrium search” in Figure 7. The final optimised geometry has, therefore, an optimum main and flap angle, and a twist profile that replicates the AWA profile at the obtained sailing conditions. The optimisation was performed applying a pattern search algorithm.

In Figure 9 and Figure 10 the convergence histories of the optimisation variables are presented. The main-element angle of attack (AoA) is defined in terms of the

wing root chord angle with respect to the boat symmetry plane. The flap angle (δ) is defined as the angle between the main and the flap chord. Figure 11 shows the maximum boat speed for each iteration.

In 10 and 15 knots of wind at 50° true wind angle, the boat sailed on the foil at 27 and 32 knots, respectively. The optimum angle of attack of the wing fore element was 4° and 3° , respectively, at the root; while the optimum flap angle with respect to the fore element was 5° and 4° , respectively. Similar boat speeds could be achieved by increasing the angle of attack of the fore element and decreasing the angle of attack of the flap, or vice versa.



Figure 8. Side view of the tested wing planform

4. CONCLUSIONS

An aerodynamic optimisation procedure for an AC72 wing sail was developed. It includes a RANS solver and a VPP. The boat performance is maximised identifying the optimum values of a set of parameters defying the wing trim. In particular, a four degrees of freedom equilibrium equation system is solved for a prescribed wing geometry, providing the sail forces by RANS computations. An optimisation algorithm guides the shape modifiers in order to drive the search by identifying the optimum wing trim for prescribed true wind conditions. The objective is to maximise the boat speed.

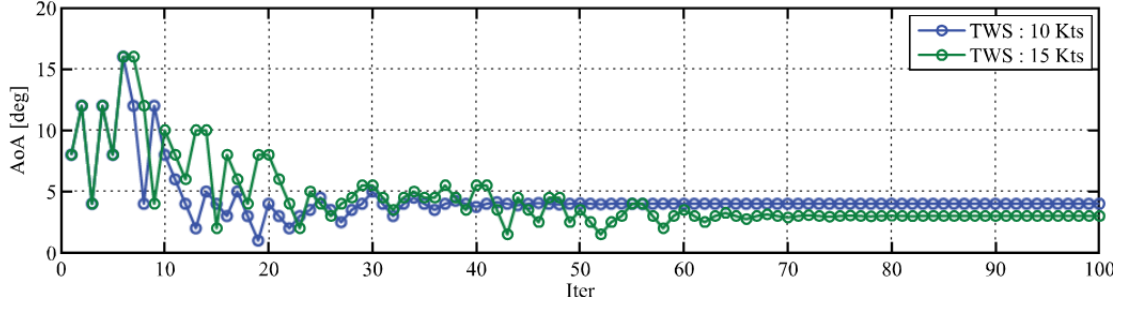


Figure 9. Convergence histories of main element angle of attack for the first set of results

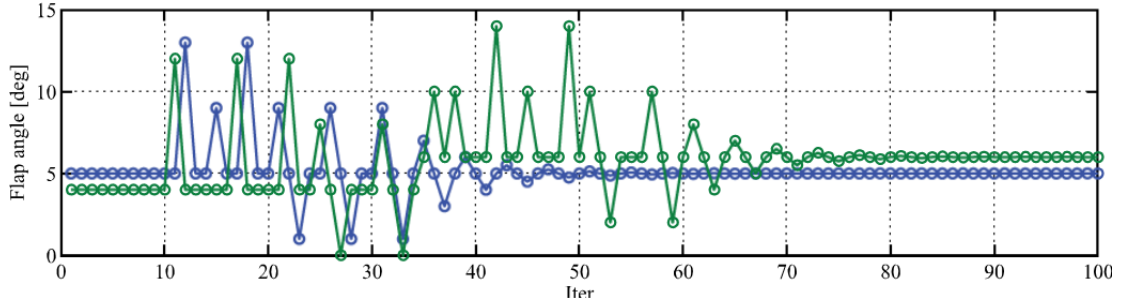


Figure 10. Convergence histories of flap element angle of attack for the first set of results

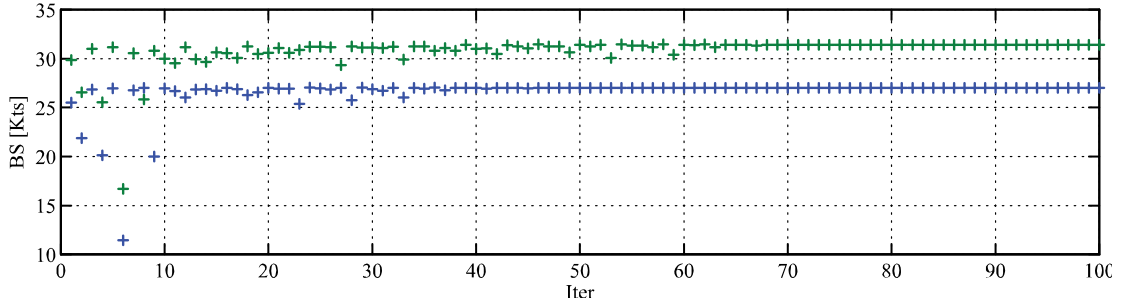


Figure 11. Convergence histories of the boat speed for the first set of results

The effectiveness of the developed code was demonstrated showing a two variable single objective optimisation. The variables were the trim angles of the two wing elements, and the angles of attack were optimised at two different true wind speeds.

While the results could not be validated due to a lack of experimental data, the computed maximum boat speed and optimum wing trim had reasonable values compared to what has been observed in full scale.

The gap between the main element of the wing and the flap was set constant to 2% of the chord. This value was found to be optimum within a preliminary parametric 2D analysis. This analysis showed that a difference of a few percent can lead to either attached flow on both the wing elements or to significant trailing edge separation on the main element and stall of the flap. Therefore future works should optimise the gap between the elements taking into account the 3D effects. Separation was also

found controllable using a flexible trailing edge of the main element, and the optimum deflection angle was found equal to approximately half of the flap deflection angle.

The novel optimisation method which is proposed in this paper can be employed for the design of wing sails and to identify optimum sailing conditions. The strength of the method is a robust and efficient mesh morphing approach that allows updating the mesh with a morphing action, which requires a very small computational effort compared to re-meshing. The robustness of the method has been demonstrated, without loss of generality, using a coarse grid and a basic hydrodynamic model.

Acknowledgements

Merfyn Owen (Owen Clarke Design) is gratefully acknowledged for his valuable comments and for contributing with examples of potential wing designs.

References

1. A. De Boer, M. S. van der Schoot and H. Bijl, (2007) "Mesh deformation based on radial basis function interpolation", *Computers & Structures*, vol. 85, no. 11–14, p. 784–795.
2. S. Jakobsson and O. Amoignon, (2007), "Mesh deformation using radial basis functions for gradient based aerodynamic shape optimization", *Computers & Fluids*, vol. 36, no. 6, p. 1119–1136.
3. D. Sieger, S. Menzel and M. Botsch, (2014) "RBF morphing techniques for simulation-based design optimization", *Engineering with Computers*, vol. 30, n. 2, pp. 161-174, April.
4. M. E. Biancolini , C. Biancolini , E. Costa, D. Gattamelata and P. P. Valentini, (2009), "Industrial application of the meshless morpher RBF morph to a motorbike windshield optimisation", *proceedings of the European automotive simulation conference (EASC)*, Munich, Germany.
5. M. E. Biancolini, (2012), "Mesh morphing and smoothing by means of radial basis functions (RBF): a practical example using fluent and RBF morph", *Handbook of research on computational science and engineering: theory and practice*, vol. 2, IGI Global.
6. M. E. Biancolini , U. Cella, G. Travostino and M. Mancini, (2013), "Shaping up – Mesh morphing reduces the time required to optimize an aircraft wing", *ANSYS Advantage Magazine*, vol. VII, no. 1.
7. M. E. Biancolini and C. Groth, (2014), "An Efficient Approach to Simulating Ice Accretion on 2D and 3D Airfoils", *Advanced Aero Concepts, Design and Operations*, Bristol, UK.
8. U. Cella and M. E. Biancolini, (2012), "Aeroelastic Analysis of Aircraft Wind-Tunnel Model Coupling Structural and Fluid Dynamic Codes", *AIAA Journal of Aircraft*, vol. 49, n. 2, pp. 407-414, March–April.
9. S. Sovani and A. Khondge, (2012), "Scaling New Heights in Aerodynamics Optimization: The 50:50:50 Method", Available: <http://www.ansys.com>.
10. D. Caridi and A. Wade, (2012), "Higher-Speed CFD", *Professional Motorsport World Magazine*, April-June.
11. G. Petrone, C. Hill and M. E. Biancolini, (2014), "Track by Track Robust Optimization of a F1 Front Wing using Adjoint Solutions and Radial Basis Functions", *44th AIAA Fluid Dynamics Conference*, Atlanta, Georgia (USA).
12. M. E. Biancolini , I. M. Viola and M. Riotte, (2014), "Sails trim optimisation using CFD and RBF mesh morphing", *Computers and Fluids*, p. 46–60, 10 April.
13. M. E. Biancolini , R. Ponzini, L. Antiga and U. Morbiducci, (2012), "A new workflow for patient specific image-based hemodynamics: parametric study of the carotid bifurcation", *Conference CompIMAGE*, Summer School held by CILEA.
14. E. Costa, M. E. Biancolini , C. Groth, U. Cella, G. Veble and M. Andrejasic, (2014), "RBF-based aerodynamic optimization of an industrial glider", *International CAE Conference*, Pacengo del Garda (VR), Italy.
15. G. P. Reina, A. Della Sala, M. E. Biancolini , C. Groth and D. Caridi, (2014), "Store Separation: Theoretical Investigation of Wing Aeroelastic Response", *4th Aircraft Structural Design Conference*, Belfast.
16. America's Cup Official Race Noticeboard, "AC72 Class Rule Version 1.1", Updated on July 16, 2012 to Incorporate Amendments 1-8, Available: <http://noticeboard.americascup.com>.
17. E. Besnard, A. Schmitz, E. Boscher, N. Garcia and T. Cebeci, (1997), "Two-Dimensional Aircraft High Lift System Design and Optimization", *36th AIAA Aerospace Sciences Meeting and Exhibit*, Reno, NV, U.S.A., AIAA 98-0123.
18. F. R. Menter, (1994), "Two-Equation Eddy-Viscosity Turbulence Models for Engineering Applications", *AIAA Journal*, August, 32(8), pp. 1598-1605.
19. I.H. Abbott and A.E. Von Doenhoff, (1959), "Theory of Wing Sections, Including a Summary of Airfoil Data", *Dover Books on Aeronautical Engineering Series*, Dover Publications.
20. J. C. Lagarias, J. A. Reeds, M. H. Wright, and P. E. Wright, (1998), "Convergence Properties of the Nelder-Mead Simplex Method in Low Dimensions", *SIAM Journal of Optimization*, Vol. 9, Number 1, pp. 112–147.
21. Audet, Charles and J. E. Dennis Jr, (2003), "Analysis of Generalized Pattern Searches", *SIAM Journal on Optimization*, Volume 13, Number 3, pp. 889–903.
22. D. E. Goldberg, (1989), "Genetic Algorithms in Search, Optimization and Machine Learning", *Addison-Wesley Reading*, Massachusetts, Jan.